Polymer Composites

WILEY | spe INSPIRING PLASTICS PROFESSIONALS

RESEARCH ARTICLE

Unidirectional CFRP Reinforcement in Buried Pipelines: Performance Limits at Strike-Slip Fault Crossings

Ercan Serif Kaya[1,2,3] | Volkan Acar[4] | Ferit Cakir[5] | Ertugrul Taciroglu[2]

[1]Department of Civil Engineering, Alanya Alaaddin Keykubat University, Antalya, Turkey | [2]Department of Civil and Environmental Engineering, University of California Los Angeles, California, USA | [3]Department of Architecture, Tokyo University of Science, Tokyo, Japan | [4]Department of Mechanical Engineering, Ataturk University, Erzurum, Turkey | [5]Department of Civil Engineering, Gebze Technical University, Kocaeli, Turkey

Correspondence: Volkan Acar (volkanacar@atauni.edu.tr)

Received: 6 October 2025 | **Revised:** 19 November 2025 | **Accepted:** 30 November 2025

Keywords: buried pipelines | composite materials | fault crossing | performance limits | unidirectional CFRP | wrapping

ABSTRACT

The mechanical behavior and seismic performance of buried pipelines have been extensively investigated in recent years. However, to the best of the author's knowledge, research studies on the performance limits of these pipelines, particularly wrapped with unidirectional carbon fiber–reinforced polymer (CFRP) remain limited. This study examines the performance limits of buried steel pipelines reinforced with unidirectional CFRP as they cross strike-slip fault lines. The investigation focuses on the influence of fault angles and evaluates the effectiveness of CFRP reinforcement under these conditions. CFRP material properties were experimentally characterized by standardized tensile and three-point bending tests. A three-dimensional finite element model was developed using ABAQUS to simulate soil-pipe interaction across fault crossing scenarios with angles ranging from 0° to 40°. The study also considers various CFRP configurations, including single-layer ($t = 1.5$ mm) and four-layer ($t = 6.0$ mm) wrappings, with fiber orientations of 0° and 90°. Damage mechanisms such as local buckling, ovalization, and composite rupture were analyzed to assess performance limits under different fault angles. The results demonstrate that even a single layer of CFRP wrapping significantly enhances the displacement capacity of the pipeline compared to conventional steel pipelines. Reinforced configurations showed reduced stress concentrations and more ductile behavior under both tensile and compressive loading. These findings offer valuable insights into optimizing CFRP retrofitting strategies and enhancing the resilience and safety of buried pipeline infrastructure in seismically active regions.

1 | Introduction

Buried pipelines are a critical part of modern infrastructure, serving as the primary means of transporting oil, gas, and water products over large distances. Ensuring the structural integrity of these systems is essential, as they play an indispensable role in supporting industrial, commercial, and residential needs, particularly in the aftermath of major seismic events. Recent earthquakes, such as the 2023 Türkiye earthquakes [1–4], the 2019 Christchurch earthquake [5], the 2016 Kumamoto earthquake [6], and the 1999 Kocaeli earthquake [7, 8], have demonstrated the profound impact of damage to pipeline systems and connected units under seismic loads. Among these seismic activities, major fault crossings pose the greatest threat to pipeline systems due to abrupt permanent ground deformation (PGD).

Design principles emphasize that pipelines should be positioned along their routes to be subject to predominantly tensile loads, thereby optimizing their structural performance and reliability [9]. However, this approach does not necessarily guarantee tension failure under combined loading conditions [10]. Such conditions can arise from fault ruptures, mapping uncertainties, and constraints imposed by forced route selection, leading to significant compressive stresses and strains that may result in premature

Highlights

- CFRP-wrapped pipelines' performance limits assessed at strike-slip fault crossings up to ±40°.
- Wrap thickness and fiber angle impact buckling, ovalization, and failure under fault movement.
- Fault-induced tension and compression behavior analyzed via calibrated 3D finite element models.
- Single-layer CFRP wrapping improves structural integrity of pipes and delays local buckling at fault crossings.
- Experimental CFRP tests enhance the accuracy of soil–pipe interaction modeling and failure prediction.

failure modes [11]. At this stage, flexible joints [12–15] and fiber-reinforced composite (FRP) wrapping [16–18] are the primary countermeasures employed to buried steel pipelines to mitigate earthquake-induced damage. However, the majority of research on FRP composite materials for steel pipes addresses corrosion repair [16] and structural strengthening [17] as well as rehabilitation [18] studies, while studies examining the impact of carbon fiber–reinforced polymer (CFRP) wrapping on steel pipes at fault crossings remain limited [19–21]. In addition to these classical applications, several recent studies have provided new insights into CFRP strengthening, composite–steel interaction, and pipeline response under extreme loading. Contemporary works have examined interfacial debonding mechanisms in FRP-strengthened steel pipes, advanced constitutive modeling for CFRP–steel systems, and the effects of CFRP retrofitting under blast, external pressure, and geohazard-induced deformation. Furthermore, recent numerical and experimental developments have significantly improved soil–pipe interaction modeling and design practices for buried pipelines. Incorporating these contemporary findings strengthens the scientific context of the present study and highlights the need for updated evaluations of CFRP-wrapped pipelines under fault-induced PGD. One of these studies examined the performance of both flexible joints and CFRP wrapping at major fault crossings, based on the real case scenario of the Thames water pipeline impacted during the 1999 Kocaeli earthquake [19]. The study highlighted that flexible joints are more effective due to their superior capacity to absorb high strain and deformation under compressive loads compared to FRP-wrapped pipelines. Additionally, it was observed that the compressive limit states were reached at an early stage of fault offsets (approximately 1.0 m) regardless of the wrapping thickness and length of layer orientation [19]. Similarly, adjusting the CFRP thickness and wrapping direction can delay the formation of local buckling to some extent; however, the limit states were still reached at fault offsets of less than 1.0 m at reversed fault movements [20].

On the other hand, CFRP wrapping significantly increased the fault displacement capacity required to induce when steel pipelines were subjected to tensile loads [21]. However, this study assumed the pipeline to be orientated perpendicular to the fault line and only considered a fault angle of 90°. Both studies employed API 5L X65 steel grade and clay soil conditions for the numerical studies, as well as the mechanical properties of the CFRP material, which were taken from literature studies [22, 23] without conducting any experimental tests. Parallel to these findings, recent advances in the broader FRP pipeline literature have revealed important insights relevant to composite strengthening but have not addressed the unique demands posed by strike-slip PGD. Interfacial behavior has been shown to play a critical role, with Wu and Chen [24] demonstrating that adhesive stiffness, bond strength, and fracture toughness govern stress transfer and debonding in FRP–steel interfaces. CFRP retrofitting has proven effective in recovering structural capacity in corrosion-damaged pipelines, as evidenced by Tabiee and Khaloo [25] under blast loading and Patnaik and Rajput [26] under subsurface explosions. Under external pressure, Alrsai et al. [27] reported significant increases in collapse and buckle propagation resistance in hybrid steel–CFRP pipes, while Shi et al. [28] developed a constitutive model capable of accurately predicting the internal-pressure behavior of steel–CFRP composite pipelines. Additionally, Soveiti and Mosalmani [29] highlighted the importance of composite lay-up and winding angle in buried composite pipelines subjected to strike-slip fault displacement. Although these studies collectively demonstrate the beneficial mechanical contributions of CFRP systems, they primarily address corrosion damage, internal or external pressure, blast loading, or fully composite pipes—leaving the performance limits of CFRP-wrapped steel pipelines under PGD insufficiently understood.

In the present study, one-layer (1.5 mm) and four-layer (6.0 mm) CFRP wrapping configurations were selected because they represent the minimum and maximum practical limits commonly used in field applications for buried steel pipeline retrofitting. Commercial CFRP systems used in pipeline rehabilitation typically employ 1–4 layers depending on available excavation width, installation constraints, and allowable stiffness modification. Intermediate configurations (2 or 3 layers) were not included to maintain a focused parametric space while still capturing the full practical strengthening range. Similarly, fiber orientations of 0° and 90° were selected as they correspond to the two principal directions governing pipeline behavior under PGD: axial stiffness (0°) controlling tensile and compressive capacity, and circumferential stiffness (90°) controlling ovalization. Off-axis orientations (e.g., ±45°) were excluded because they primarily affect shear coupling rather than the dominant axial–circumferential mechanisms relevant to strike-slip fault crossings.

These recent studies have been integrated into the revised manuscript to ensure that the research is positioned within the most up-to-date scientific framework. In contrast to previous studies, the present research incorporates experimentally measured mechanical properties of the CFRP system, enabling more realistic simulation of composite damage initiation and progression. In addition, a fully three-dimensional nonlinear soil–pipe interaction framework is developed to evaluate pipeline behavior over a broad range of fault-crossing angles (−40° to +40°), rather than a single or limited fault configuration. A unified limit-state assessment methodology is also introduced, simultaneously addressing local buckling, ovalization, and CFRP rupture. Parametric variations of wrap thickness and ply orientation are further examined to clarify their influence on fault-induced deformation capacity. These theoretical and methodological developments collectively extend the existing literature and provide a more comprehensive understanding of CFRP-wrapped pipeline performance under PGD conditions.

2 | Limit States for Steel Pipes

The performance criteria for buried pipelines are mainly assessed based on various damage types, including:

a. The allowable maximum tensile and compressive strain, which points out the onset of local buckling as defined by various regulations.
b. The degree of cross-sectional ovalization of the pipe.
c. The rupture of the composite wrapping (if FRP wrapping is applied).

The critical fault offset corresponding to the onset of buckling will be calculated according to the specified maximum tensile and compressive strain values given in Table 1.

2.1 | Tensile and Compressive Limit Strains

Tensile and compressive limit stresses indicate the amount of damage limited by regulations, mainly caused by spatially varying or abrupt permanent soil deformations. For tension-controlled and compression-controlled ruptures, various strain limits are suggested and the majority of these regulations, such as ALA2005 [30] and PRCI [31], identify two limit states: normal operability and pressure integration. Wijewickreme et al. [32] also proposed given strain equations corresponding to 10% and 90% probability of limit states (Table 1).

TABLE 1 | Limit states for buried steel pipes due to permanent ground deformation, including earthquake or landslides.

Tensile strain	Compressive strain (local buckling)
ALA 2005 [30]	**ALA 2005 [30]**
2% (normal operation)	Special equation 4.9
4% (pressure integrity)	1.76 t/D (pressure integrity)
PRCI 2004 [31]	**PRCI 2004 [31]**
1%–2% (normal operation)	Special equation 4.13 or 4.14
2%–4% (pressure integrity)	1.76 t/D (pressure integrity)
Wijewickreme et al. 2005 [32]	**Wijewickreme et al. 2005 [32]**
3% (10% probability of failure)	0.4 t/D (10% probability of failure)
10% (90% probability of failure)	2.4 t/D (90% probability of failure)

2.2 | Pipe Ovalization

The ovalization limit state quantifies the cross-sectional distortion using the flattening parameter, f, as defined by Gresnigt et al. [33]. According to this criterion, a pipe is considered to have reached its ovalization limit state when the ratio of the deformed pipe diameter (ΔD) to the original diameter (D) reaches 0.15 (i.e., the deformed diameter becomes 0.85D) (Figure 1).

2.3 | Unidirectional CFRP Rupture

The limit state of composite material rupture can be reached due to the transverse distortion of the pipes (ovalization). In the developed finite element model, the steel pipe and its composite wrap are assumed to undergo identical deformation and strain, based on the assumption of a perfect bond between them that prevents any slippage. And the ultimate tensile strain for the composite material is taken as 0.049 ± 0.005 according to the experimental work carried out in the next section, by using the average of 8 test specimens (Figure 3).

3 | Experimental Procedure

In the study, the Kratos C-Plate—a commercial unidirectional (UD) carbon-fiber-reinforced epoxy composite manufactured by Kordsa Inc. (Kocaeli, Türkiye)—was used [34]. Mechanical characterization of the composite material was conducted using a universal mechanical testing machine with a 100 kN load capacity (Ag-IS, Shimadzu Corp., Japan). All specimens were cut to the required dimensions using a precision diamond saw to avoid inducing thermal or mechanical damage along the edges, and their surfaces were cleaned with isopropyl alcohol to ensure consistent gripping conditions. Tensile tests were performed in accordance with ASTM D3039 [35]. End tabs were bonded to both ends of each specimen to prevent gripping-induced premature failures, and a clip-on extensometer was attached to the gauge region for strain measurements. Eight tensile specimens

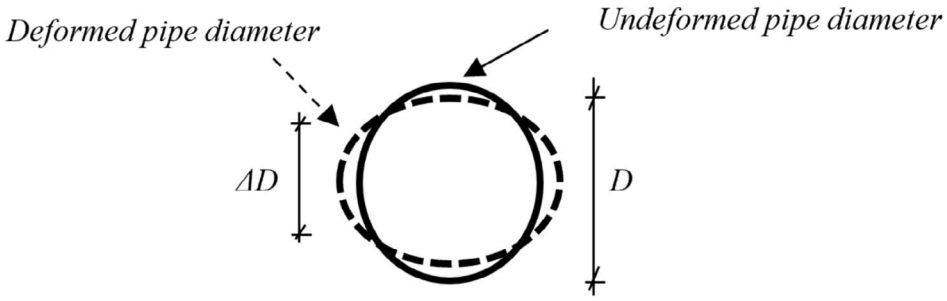

FIGURE 1 | Cross-sectional ovalization.

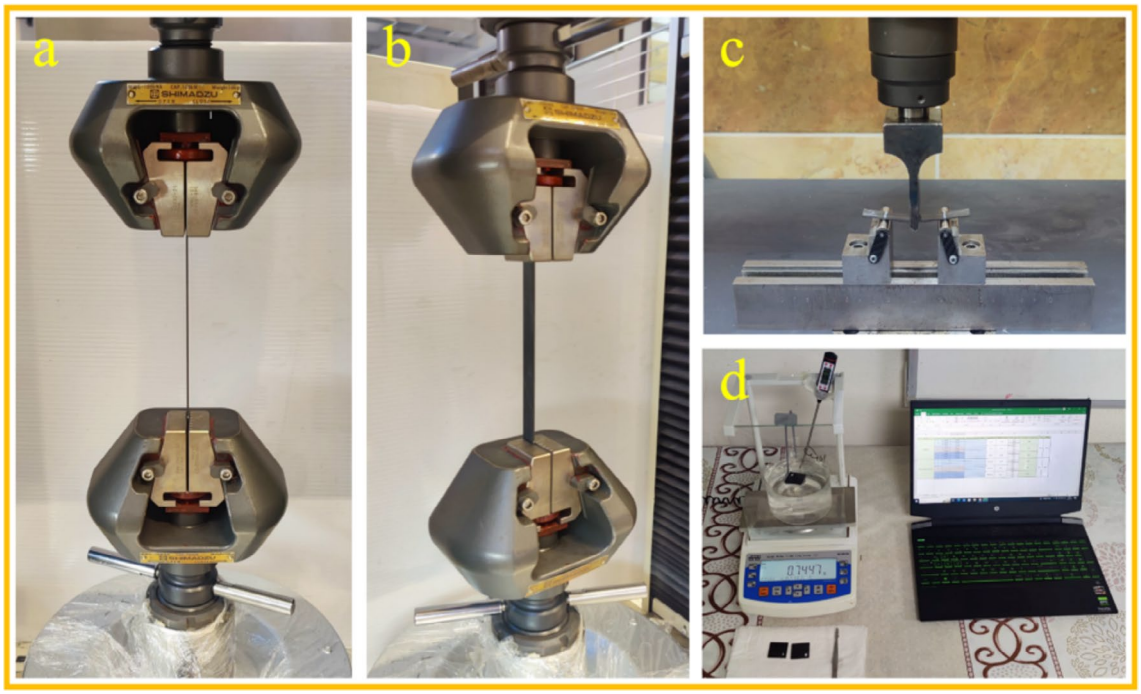

FIGURE 2 | (a) Tensile test (front view), (b) tensile test (isometric view), (c) three-point bending test, and (d) density measurement setup.

were tested at room temperature under displacement control at a loading rate of 1 mm/min. The tensile test rig is illustrated in Figure 2a (front view) and Figure 2b (isometric view), showing the alignment fixtures, extensometer placement, and the specimen configuration used during testing.

Flexural behavior was evaluated using three-point bending tests in accordance with ASTM D790 [36]. Twelve specimens were tested at a displacement rate of 1 mm/min, using a span-to-depth ratio of 16:1 in compliance with standard requirements. Mid-span deflections were measured using an integrated LVDT. The experimental setup for three-point bending is presented in Figure 2c, which shows the loading nose, supports, and measurement arrangement. Additionally, the density of the composite material was determined following ASTM D792 [37] using a precision analytical balance and distilled water as the immersion medium. The density measurement setup is shown in Figure 2d, including the immersion basket and balance configuration used to compute the composite's specific gravity and verify material consistency. After each test, fracture surfaces were documented using high-resolution photographs to identify governing failure mechanisms such as fiber rupture, matrix cracking, interlaminar shear, and delamination. The experimentally obtained parameters (including longitudinal elastic modulus, flexural modulus, shear modulus, Poisson's ratios, and tensile/flexural strength values) were subsequently used to define the orthotropic elastic behavior and damage initiation parameters of the CFRP material in the finite element model described in the following sections.

Table 2 shows the mechanical properties of the composite specimen used in the study. Figure 3 shows representative strain curves corresponding to tensile and flexural stresses. Figure 4 shows images of the fractured specimen subjected to the tensile test. Since the composite product was offered for sale in 100 mm width, it was not possible to perform tensile tests in the transverse direction. Therefore, the mechanical properties in the transverse direction and Poisson's ratio values were obtained from similar composites in the literature, and numerical analysis was performed [38, 39].

4 | Finite Element Modeling

A three-dimensional numerical model, developed in association with the framework presented in [40], is employed to evaluate the structural response of a buried steel pipeline at a fault crossing following calibration studies. The analysis is conducted using the finite element software ABAQUS. The comprehensive soil-pipe model (Figure 5) incorporates solid elements (C3DR8) to represent the surrounding soil blocks, each measuring 30.0 m, and shell elements (S4R) for the steel pipeline, extending 60.0 m (Figure 5). The width and the burial depth of the soil block are assumed to be equal to 10.0 (10.0*D*) and 2.5 (2.5*D*) times of the pipe diameter, respectively. The modeling strategy employed in this study represents an advancement over previous approaches by integrating experimentally calibrated CFRP constitutive properties with a fully nonlinear soil–pipe interaction model. The model framework simultaneously captures soil plasticity, pipeline ovalization, composite damage progression through Hashin criteria, and fault-induced axial deformation patterns across multiple fault angles. The two CFRP thicknesses examined (1.5 and 6.0 mm) were chosen to represent the lower and upper bounds of practical retrofit applications reported in the industry and manufacturer datasheets. Likewise, only 0° and 90° ply orientations were modeled because they represent the principal stiffness directions that govern axial strain development, local buckling, and ovalization during fault-induced deformation. This selection ensures that the parametric study directly targets the dominant mechanical mechanisms relevant to fault crossing behavior without introducing additional variables that have limited influence on the primary response modes. The

TABLE 2 | Materials properties of unidirectional carbon fiber reinforced epoxy composites.

Material properties	Symbol	Values
Longitudinal modulus (GPa)	E_{11}	165.00
Transverse modulus (GPa)	$E_{22}=E_{33}$	9.00
Shear modulus (GPa)	$G_{12}=G_{13}$	5.00
Shear modulus (GPa)	G_{23}	3.00
Poisson's ratio	$\nu_{12}=\nu_{13}$	0.28
Poisson's ratio	ν_{23}	0.40
Longitudinal tensile strength (MPa)	X_T	1623.19
Longitudinal compression strength (MPa)	X_C	1197.00
Transverse tensile strength (MPa)	$Y_T=Z_T$	48.00
Transverse compression strength (MPa)	$Y_C=Z_C$	200.00
Shear strength (MPa)	$S_{12}=S_{13}$	79.00
Shear strength (MPa)	S_{23}	42.00
Specific tensile strength (MPa/g cm^{-3})	X^*_T	1033.88
Specific modulus (GPa/g cm^{-3})	E^*_{11}	29.85
Flexural strength (MPa)	X_F	1156.38
Flexural modulus (GPa)	E_F	54.29
Specific flexural strength (MPa/g cm^{-3})	X^*_F	736.55
Specific flexural modulus (GPa/g cm^{-3})	E^*_F	34.58
Density (g/cm^3)	ρ	1.57
Fiber volume fraction (%)	V_f	60.00

dimensions of the soil domain were selected following the recommendations of Vazouras et al. [40], who demonstrated that a soil block extending approximately 30 m longitudinally and 30 m transversely from the pipeline is sufficient to eliminate boundary-induced stiffness effects for strike-slip faulting scenarios. In accordance with their findings, the soil domain in the present study was modeled as a 30 m × 30 m block with a burial depth of approximately 2.5D, ensuring that wave reflections and constraint interactions from the outer boundaries did not affect the pipeline response (Figure 5). Trial analyses confirmed that further enlargement of the soil domain resulted in changes of less than 1% in peak axial strain and ovalization values, verifying that the chosen boundaries were sufficiently remote to avoid artificial confinement. This mesh and soil domain configuration is consistent with the modeling strategy employed by Vazouras et al. [40], who also demonstrated that boundary distances exceeding 30–50 m are sufficient to prevent numerical confinement effects in strike-slip fault analyses.

The pipe has a diameter of 914.4 mm and a wall thickness of 12.57 mm with the mechanical properties of grade X65 steel. The Mohr–Coulomb material plasticity for the soil condition is defined as medium clay soil parameters with Young's modulus of $E=25$ MPa, poison's ratio of $\nu=0.45$, cohesion of $c=50.0$ kPa and density of $\gamma=1.85$ tons/m^3.

The pipeline crosses the fault line at different fault angles (β) in a range of ±40°. The fault line is perpendicular to the pipe axis when the fault angle is equal to 0°, meaning that both left, and right lateral strike-slip fault movements result in tensile loads acting along the pipe. As the fault angle increases, left and right lateral strike-slip can cause either tensile or compressive loads, depending on the fault angle and type (Figure 6). For example, a pipe crossing the fault line with $\beta=30°$ subjected to compressive loads during right lateral and tensile loads during left lateral strike-slip fault movements.

Carbon fiber-reinforced composite (CFRP) material is also modeled as shell elements (S4R) according to the Hashin damage model parameters obtained experimentally. The adhesive behavior between the pipe surface and CFRP wrapping is defined

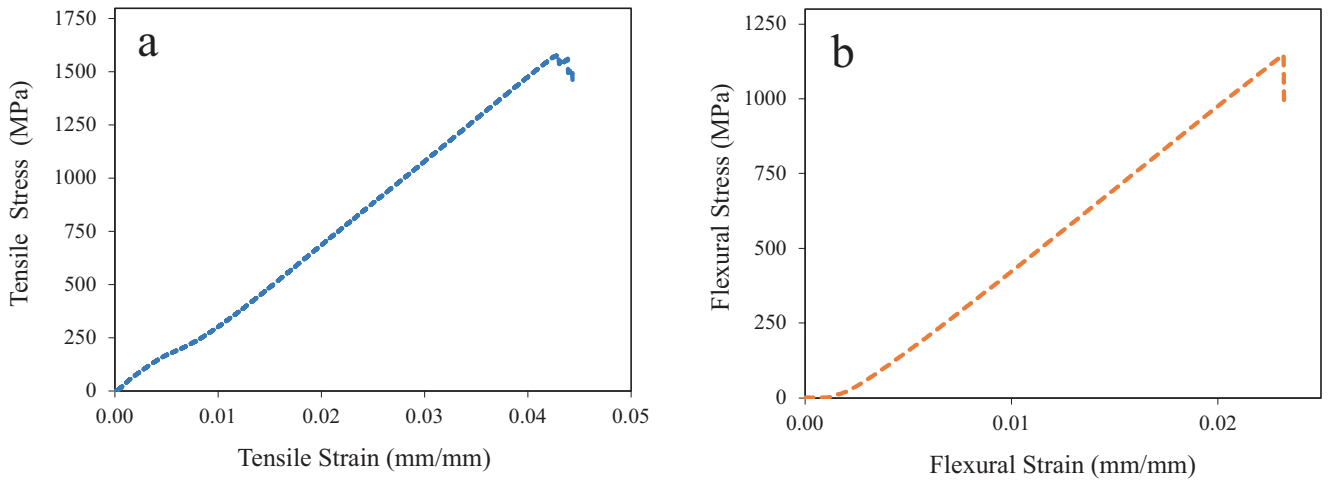

FIGURE 3 | (a) A representative tensile stress—tensile strain curve and (b) a representative flexural stress—flexural strain curve of the composites.

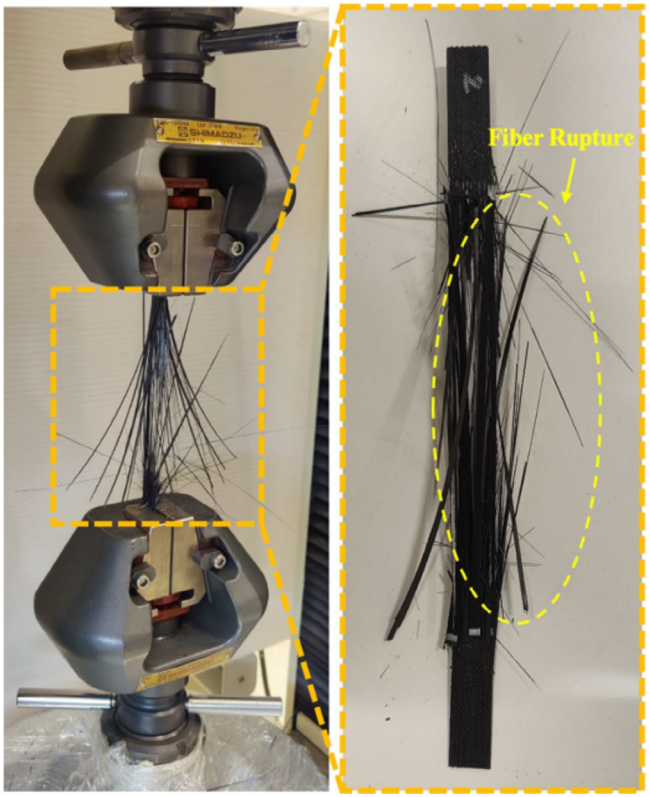

FIGURE 4 | A fractured tensile test specimen.

perfectly through tie constraint between these two surfaces. Two sets of wrapping thicknesses are defined through one and four layers (each layer has a thickness of 1.5 mm) of ply stack using 0° (parallel to the pipe axis) and 90° (parallel to the fault line) degrees of stack orientations (Figure 7). The length of the CFRP wrapping is set to 20.0 m to ensure coverage of the effective length of the pipe.

All other assumptions, such as boundary conditions, contact algorithm defined between soil and pipe surfaces, gravitational and quasi-static loading protocols, are made in accordance with the literature studies [41, 42].

5 | Results and Discussion

In this study, a wide range of fault transition angles ranging from ±40° was considered in the analyses, and comparative analyses of conventional (unwrapped) steel pipes with steel pipes reinforced with various CFRP wrapping configurations were performed. In Figure 8, the normalized fault displacements for both conventional steel pipes without CFRP and CFRP-wrapped steel pipes are presented for each fault crossing angle, ranging between −40° and 40°, corresponding to the 2.0% (green dotted line) and 5.0% (red dotted line) strain limit values. The conventional steel pipe reaches its 2% and 5% of strain values at approximately 1.0 and 2.0 times of the normalized fault displacements, respectively. However, applying

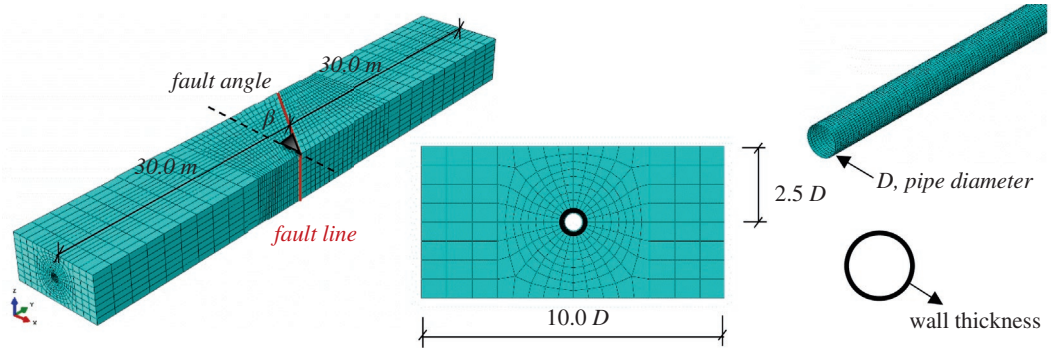

FIGURE 5 | Soil–pipe interaction model.

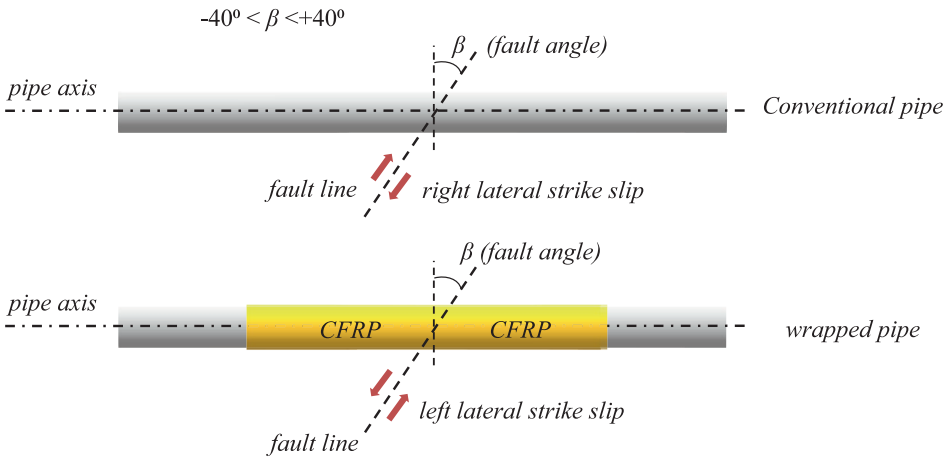

FIGURE 6 | Different fault-crossing scenarios affecting the forces acting along the pipe.

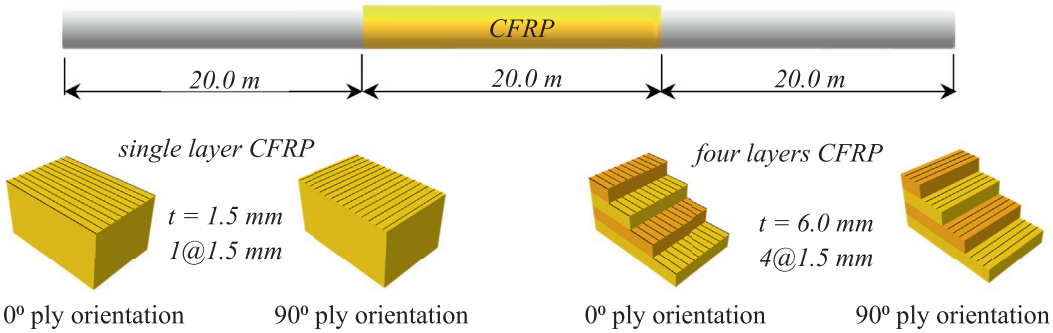

FIGURE 7 | CFRP-wrapping configuration used in the steel pipe.

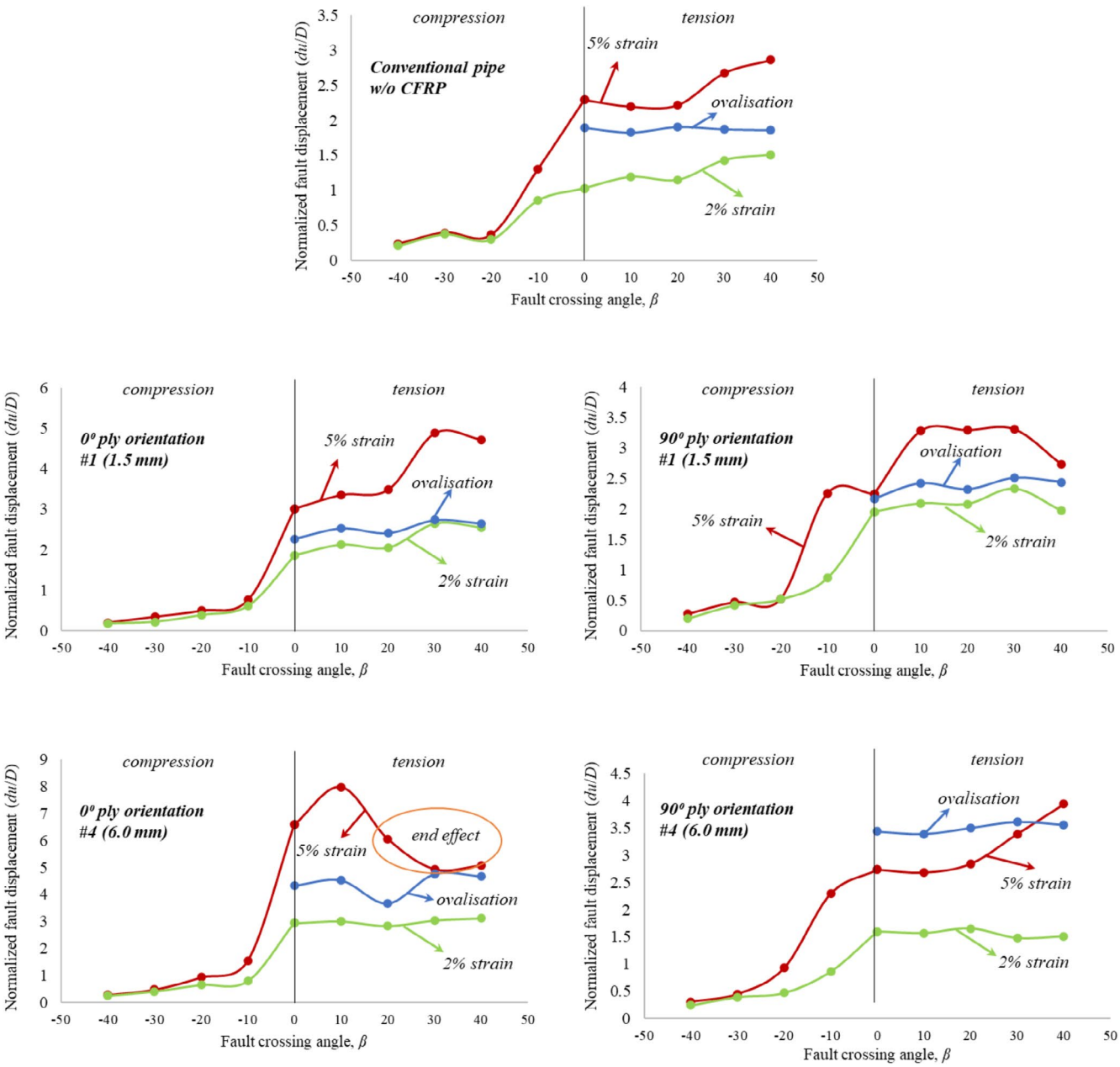

FIGURE 8 | Normalized critical fault displacement for various performance limits at different fault crossing angles for different CFRP configurations of the pipeline.

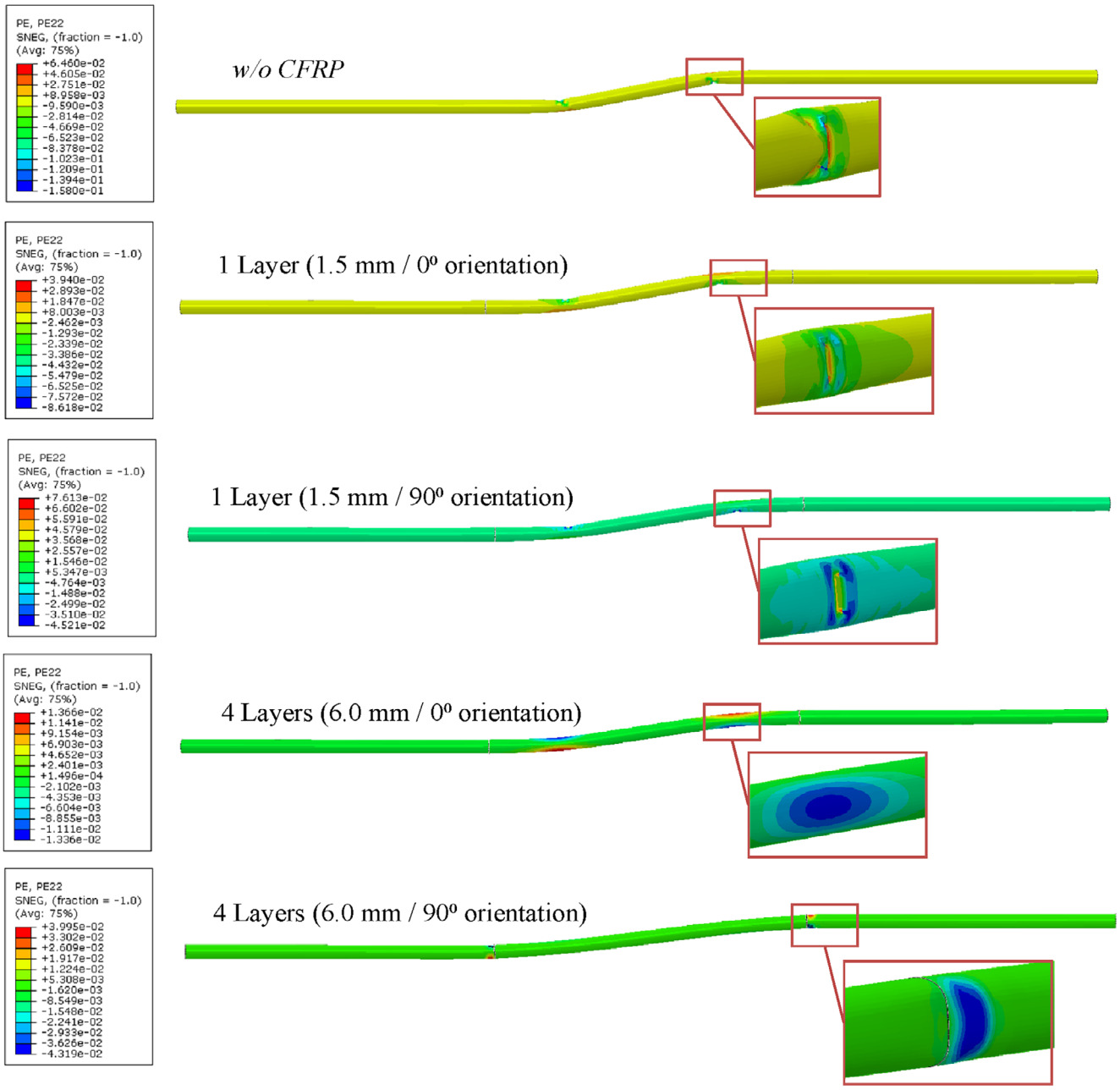

FIGURE 9 | Axial plastic strain values at 2.0 m fault offset (fault angle, $\beta = 0°$).

even a single layer (1.5 mm) of composite material to the conventional steel pipe effectively doubles these values both for 0° and 90° ply-oriented composites. These results provided comprehensive insights into the effect of CFRP wrapping on the fault displacement capacity of buried steel pipelines. These results collectively indicate that CFRP wrapping can significantly improve the resistance of buried steel pipelines subjected to seismic ground motions. The interaction between wrap thickness and ply orientation emerges as a decisive factor in tailoring the reinforcement strategy to specific fault-crossing scenarios. While a single layer of CFRP offers a significant performance enhancement, an optimized multilayer system not only further increases the displacement capacity but also promotes a more favorable, ductile failure progression. This is particularly important in seismic regions where sudden ground deformations can lead to catastrophic pipeline failures. Furthermore, integrated experimental and numerical findings confirm the effectiveness of CFRP wrapping as a robust strengthening solution for buried pipelines. By effectively doubling, in some cases significantly increasing, the fault displacement capacity, the application of CFRP reinforcement offers a viable strategy to enhance the structural integrity and operational safety of pipeline infrastructures in earthquake-prone regions. The insights gained from this study pave the way for developing refined design guidelines incorporating advanced composite materials to mitigate the adverse effects of seismic activity on critical infrastructure.

Analyzing the obtained results in terms of damage mechanisms, under tensile loading conditions, especially at a fault angle of +40°, the CFRP wrap made the peak plastic strains more diffused and reduced along the critical sections

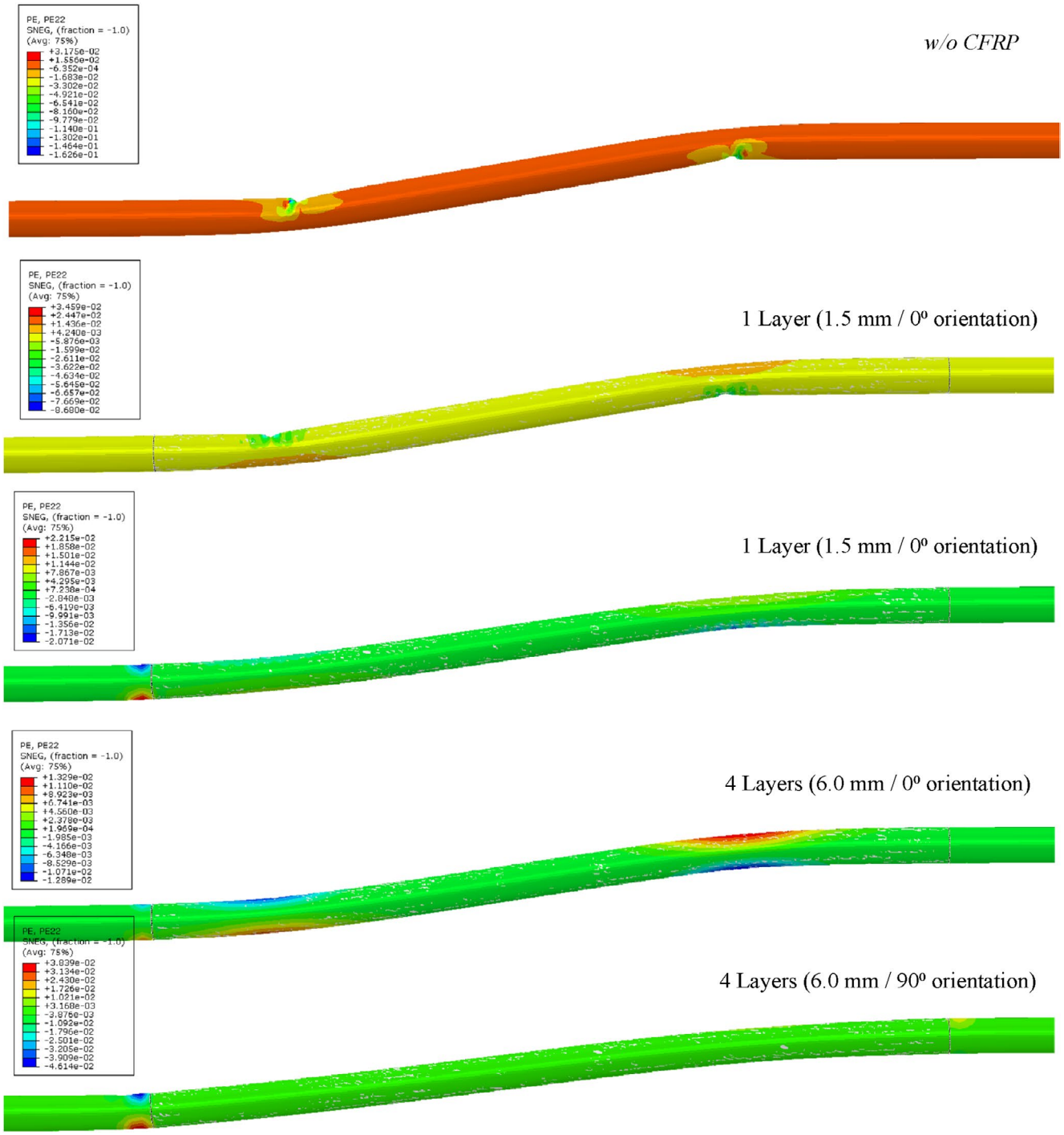

FIGURE 10 | Axial plastic strain values at 2.0 m fault offset under tension (fault angle, $\beta = +40°$).

of the pipeline. This strain attenuation delayed the onset of damage mechanisms and thus extended the operational displacement range. Conversely, under compressive conditions at smaller fault distances (e.g., 0.20 m), the wrapping introduced additional stiffness that restricted the rapid development of localized plasticity, thus increasing the resistance of the pipeline to early buckling. The performance gains were even more pronounced when thicker CFRP configurations were used, particularly a four-layer system corresponding to a thickness of 6.0 mm. Under these conditions, the failure mode showed a shift toward more ductile behavior, in some cases from local buckling to ovalization or CFRP end-effect buckling. For example, under tensile loads at a fault angle of +40°, conventional steel pipe exhibited early-onset local buckling, while CFRP-wrapped pipelines maintained structural integrity over wider displacement ranges. Similarly, under compressive conditions at lower fault distances, CFRP wrapping effectively reduced the concentration of axial plastic stresses, thus delaying the progression toward critical damage (Figures 9–11).

A detailed comparison between various fault angles revealed a more pronounced contribution to the wrap configuration. At fault angles close to 0° and 10°, both 0° and 90° ply orientations

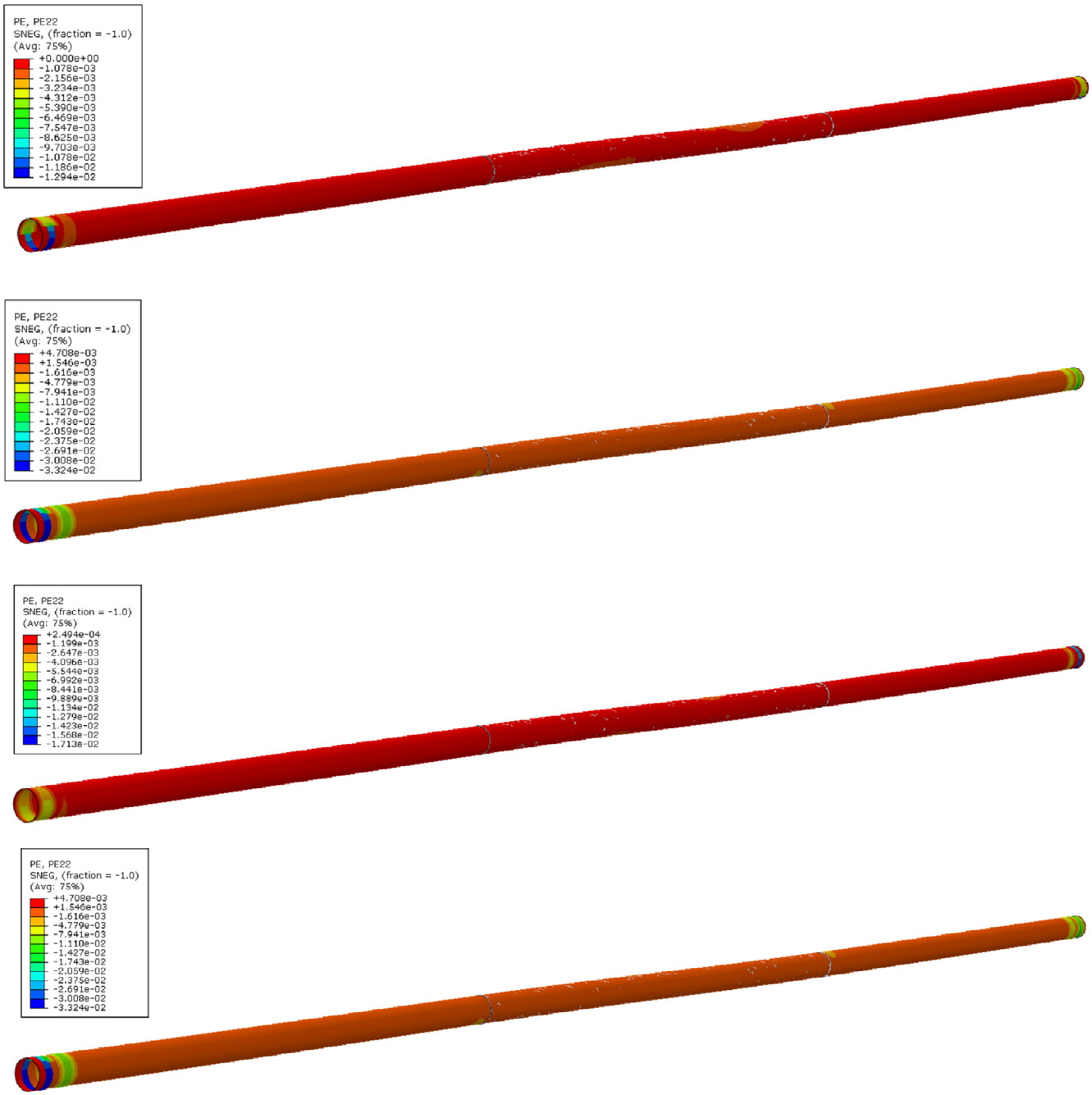

FIGURE 11 | Axial plastic strain values at 0.20 m fault offset under compression ($\beta = \pm 40°$).

in a single-layer configuration showed displacement capacity increases exceeding 80%–100% compared to the unwrapped case. As the fault angle increased to 20° and beyond, performance continued to improve, although the relative percentage increase in capacity varied depending on the dominant loading regime (tensile or compression) and the associated failure criterion (local buckling versus ovalization). In some cases, the four-layer wrap configuration provided displacement capacity improvements of up to 447% when evaluated against the ovalization limit state, demonstrating the critical importance of composite thickness in improving the overall ductility and deformation properties of the pipeline (Table 3). Table 3 presents the limit state criteria, d_{cr} (m), and percentage increase for different fault angles (β), CFRP thicknesses (t), and layer orientations, showcasing the effects of CFRP (carbon fiber-reinforced polymer) reinforcement on local buckling, ovalization, and CFRP end effect buckling under various conditions. At a 0° fault angle, without CFRP reinforcement, local buckling occurs with a d_{cr} of 0.76 m. Introducing 1.5 mm CFRP at a 0° layer orientation results in local buckling with a d_{cr} of 1.51 m, marking a 108% increase, whereas with 6.0 mm CFRP, ovalization occurs with a d_{cr} of 3.95 m, a 447% increase. For a 10° fault angle, the d_{cr} values without CFRP reinforcement are 0.96 m, but with 1.5 mm CFRP at 0° orientation, local buckling results in a d_{cr} of 1.77 m, an 84% increase, while 6.0 mm CFRP leads to ovalization with a d_{cr} of 4.13 m, a 330% increase. At a

TABLE 3 | Limit states and critical displacements for different CFRP wrapped pipe configurations at different failure angles.

Fault angle (β)	CFRP thickness (t)	Layer orientation (°)	Limit state criterion	d_{cr} (m)	Increase (%)
0°	0	W/o CFRP	Local buckling	0.76	—
	1.5 mm	0	Local buckling	1.51	108
		90	Local buckling	1.83	129
	6.0 mm	0	Ovalization	3.95	447
		90	CFRP end effect buckling	2.45	222
10°	0	W/o CFRP	Local buckling	0.96	—
	1.5 mm	0	Local buckling	1.77	84
		90	Local buckling	2.14	123
	6.0 mm	0	Ovalization	4.13	330
		90	CFRP end effect buckling	2.21	130
20°	0	W/o CFRP	Local buckling	1.09	—
	1.5 mm	0	Local buckling	1.71	57
		90	Local buckling	1.97	81
	6.0 mm	0	Local buckling	2.92	168
		90	CFRP end effect buckling	2.39	119
30°	0	W/o CFRP	Local buckling	1.13	—
	1.5 mm	0	Local buckling	2.13	89
		90	Local buckling	2.10	86
	6.0 mm	0	CFRP end effect buckling	4.27	278
		90	CFRP end effect buckling	2.07	83
40°	0	W/o CFRP	Local buckling	1.18	—
	1.5 mm	0	Local buckling	1.77	50
		90	Local buckling	2.05	74
	6.0 mm	0	CFRP end effect buckling	3.75	218
		90	CFRP end effect buckling	2.26	92

20-degree fault angle, local buckling without CFRP results in a d_{cr} of 1.09 m. However, with 1.5 mm CFRP at 0-degree orientation, local buckling yields a d_{cr} of 1.71 m, reflecting a 57% increase, and with 6.0 mm CFRP, local buckling shows a d_{cr} of 2.92 m, marking a 168% increase. For a 30-degree fault angle, local buckling occurs with a dcr of 1.13 m without CFRP reinforcement, while 1.5 mm CFRP at 0-degree orientation results in local buckling with a d_{cr} of 2.13 m, an 89% increase, and with 6.0 mm CFRP, CFRP end effect buckling occurs with a d_{cr} of 4.27 m, reflecting a 278% increase. At a 40-degree fault angle, local buckling occurs with a d_{cr} of 1.18 m without CFRP reinforcement, whereas 1.5 mm CFRP at 0-degree orientation results in local buckling with a d_{cr} of 1.77 m, a 50% increase, and with 6.0 mm CFRP, CFRP end effect buckling occurs with a d_{cr} of 3.75 m, marking a 218% increase. The table indicates that as CFRP thickness increases and layer orientation changes, significant increases in buckling and ovalization are observed, suggesting that CFRP reinforcement enhances structural performance.

6 | Conclusions

In conclusion, this study shows that CFRP reinforcement significantly improves the structural performance of buried steel pipelines when passing through active fault zones. The analysis, supported by experimental characterization studies and numerical simulations, reveals that the use of CFRP wrapping, even with a single layer, almost doubles the displacement capacity of pipelines compared to conventional steel pipes. The results show that different CFRP layer thicknesses at the same fault angle have a significant effect on the structural performance. For example, at 0° failure angle, the local buckling without CFRP reinforcement is 0.76 m d_{cr}, while with CFRP reinforcement of 1.5 mm thickness, this value increases to 1.51 m, showing an increase of 108%. At 6.0 mm thickness, the ovalization is 3.95 m d_{cr}, an increase of 447%.

Similarly at 10° failure angle, without CFRP reinforcement, the local buckling is 0.96 m d_{cr}, at 1.5 mm thickness 1.77 m

d_{cr} (84% increase) and at 6.0 mm thickness the ovalization is 4.13 m d_{cr} (330% increase). Similarly, for other failure angles, significant increases in local buckling, ovalization and CFRP end-effect buckling are observed with increasing CFRP thickness.

These data indicate that increasing the CFRP layer thickness at the same failure angle plays a critical role in improving the structural performance. As the layer thickness increases, the resistance of the structure to buckling and ovalization increases significantly, clearly demonstrating that CFRP reinforcement improves the structural performance. The study also introduces a novel integrated limit-state evaluation method and utilizes experimentally derived CFRP material parameters, thereby enhancing the theoretical robustness and practical applicability of numerical assessments for buried pipelines subjected to strike-slip faulting.

Author Contributions

Ercan Serif Kaya: conceptualization, software, methodology, investigation, data curation, formal analysis, writing – original draft, writing – review and editing, visualization. **Volkan Acar:** conceptualization, investigation, methodology, data curation, formal analysis, visualization, writing – original draft, writing – review and editing. **Ferit Cakir:** conceptualization, methodology, software, validation, investigation, writing – review and editing, writing – original draft, supervision. **Ertugrul Taciroglu:** supervision, writing – review and editing, conceptualization, methodology, validation.

Funding

The authors have nothing to report.

Conflicts of Interest

The authors declare no conflicts of interest.

Data Availability Statement

The data that support the findings of this study are available from the corresponding author upon reasonable request.

References

1. E. Uckan, M. Aksel, O. Atas, et al., "The Performance of Transmission Pipelines on February 6th, 2023 Kahramanmaras Earthquake: A Series of Case Studies," *Bulletin of Earthquake Engineering* 23, no. 3 (2025): 1203–1223.

2. A. C. Saka, E. S. Kaya, and E. Uckan, "Seismic Performance of Cylindrical Liquid Storage Tanks in the 2023 Kahramanmaras Earthquakes: A Case Study of a Self-Supported Oil Storage Tank," *Journal of Earthquake Engineering* (2024): 1–12.

3. S. Toprak, B. P. Wham, E. Nacaroglu, et al., "Performance of Water Systems During the February 6th Kahramanmaras Earthquakes," *Earthquake Spectra* 41, no. 1 (2024): 322–353.

4. S. Toprak, B. P. Wham, E. Nacaroglu, M. Ceylan, O. Dal, and A. E. Senturk, "Impact of Seismic Geohazards on Water Supply Systems and Pipeline Performance: Insights From the 2023 Kahramanmaras Earthquakes," *Engineering Geology* 340 (2024): 107681.

5. T. D. O'Rourke, S.-S. Jeon, S. Toprak, et al., "Earthquake Response of Underground Pipeline Networks in Christchurch, NZ," *Earthquake Spectra* 30, no. 1 (2014): 183–204.

6. B. P. Wham, S. Dashti, K. Franke, R. Kayen, and N. K. Oettle, "Water Supply Damage Caused by the 2016 Kumamoto Earthquake," *Lowland Technology International* 19, no. 3 (2017): 165–174.

7. E. S. Kaya, E. Uckan, M. J. O'Rourke, et al., "Failure Analysis of a Welded Steel Pipe at Kullar Fault Crossing," *Engineering Failure Analysis* 71 (2017): 43–62.

8. J. M. Eidinger, M. O'Rourke, and J. Bachhuber, "Performance of Pipelines at Fault Crossings," in *Proceedings of the 7th US National Conference of Earthquake Engineering* (Earthquake Engineering Research Institute (EERI), 2002), 21–25.

9. E. Uckan, B. Akbas, E. S. Kaya, et al., "Design Issues of Buried Pipelines at Permanent Ground Deformation Zones," *Disaster Science and Engineering* 2 (2016): 53–58.

10. E. S. Kaya, "Determination of Performance Criteria of Steel Pipes Subjected to Axial Compressive Load and Bending Moment," *Journal of the Faculty of Engineering and Architecture of Gazi University* 38, no. 4 (2013): 2107–2118.

11. E. S. Kaya, E. Uckan, and E. Taciroglu, "Damage Mitigation of Fault-Crossing Elbowed Water Transmission Pipes Using Flexible Joints," *Soil Dynamics and Earthquake Engineering* 200 (2026): 109845.

12. A. I. Valsamis, G. D. Bouckovalas, and C. J. Gantes, "Alternative Design of Buried Pipelines at Active Fault Crossings Using Flexible Joints," *International Journal of Pressure Vessels and Piping* 180 (2020): 104038.

13. A. I. Valsamis and G. D. Bouckovalas, "Analytical Methodology for the Verification of Buried Steel Pipelines With Flexible Joints Crossing Strike-Slip Faults," *Soil Dynamics and Earthquake Engineering* 138 (2020): 106280.

14. H. Nakazono, N. Hasegawa, B. P. Wham, et al., "Innovative Solution to Large Ground Displacement Using Steel Pipe for Crossing Fault," *Pipelines* 2019 (2019): 334–345.

15. B. P. Wham, T. D. O'Rourke, H. E. Stewart, T. K. Bond, C. Pariya-Ekkasut, and H. Hall, "Large-Scale Testing of JFE Steel Pipe Crossing Faults: Testing of SPF Wave Feature to Resist Fault Rupture," 2016 (Final Report Submitted to: JFE Engineering Corporation, Connell University, 2016).

16. J. Chen, H. Wang, M. Salemi, and P. N. Balaguru, "Finite Element Analysis of Composite Repair for Damaged Steel Pipeline," *Coatings* 11, no. 3 (2021): 301.

17. K. S. Lim, S. N. Azraai, N. Yahaya, et al., "Behaviour of Steel Pipelines With Composite Repairs Analysed Using Experimental and Numerical Approaches," *Thin-Walled Structures* 139 (2019): 321–333.

18. J. M. George, M. Kimiaei, M. Elchalakani, and S. Fawzia, "Experimental and Numerical Investigation of Underwater Composite Repair With Fibre Reinforced Polymers in Corroded Tubular Offshore Structural Members Under Concentric and Eccentric Axial Loads," *Engineering Structures* 227 (2021): 111402.

19. E. S. Kaya, "Earthquake Damage Mitigation Methods for Buried Pipelines Under Compressive Loads: A Case Study of the Thames Water Pipeline," *International Journal of Pressure Vessels and Piping* 212 (2024): 105322.

20. Z. Zhong, X. Zhao, J. Cui, X. Zhao, and X. du, "Performance Assessment of Buried Steel Pipelines Reinforced With Carbon Fibre-Reinforced Polymer Under Reverse Fault Movement," *Tunnelling and Underground Space Technology* 141 (2023): 105370.

21. M. Mokhtari and A. Alavi Nia, "The Influence of Using CFRP Wraps on Performance of Buried Steel Pipelines Under Permanent Ground Deformations," *Soil Dynamics and Earthquake Engineering* 73 (2015): 29–41.

22. X. Wang, Y. Yang, R. Yang, and P. Liu, "Experimental Analysis of Bearing Capacity of Basalt Fiber Reinforced Concrete Short Columns Under Axial Compression," *Coatings* 12, no. 5 (2022): 654.

23. M. Naderi and A. R. Maligno, "Fatigue Life Prediction of Carbon/Epoxy Laminates by Stochastic Numerical Simulation," *Composite Structures* 94, no. 3 (2012): 1052–1059.

24. J. Wu and J.-F. Chen, "A Theoretical Study of Interfacial Debonding in FRP-Strengthened Steel Pressure Pipelines," *International Journal of Pressure Vessels and Piping* 218 (2025): 105622.

25. M. Tabiee and A. Khaloo, "Investigation of Corrosion Effects on the Performance of Underground Steel Pipelines Under Blast Loading and a Solution for Retrofitting," *International Journal of Pressure Vessels and Piping* 219 (2026): 105669.

26. G. Patnaik and A. Rajput, "Safety Assessment of Underground Steel Pipelines With CFRP Protection Against Subsurface Blast Loading," *Structure* 54 (2023): 1541–1559.

27. M. Alrsai, A. Alsahalen, H. Karampour, H. Alsanat, H. Guan, and H. Lin, "Experimental and Analytical Evaluation of the Performance of Hybrid Steel-CFRP Pipelines at High External Pressures," *Engineering Structures* 304 (2024): 117669.

28. J. Shi, W. Wang, W. Wei, and B. Jia, "Calculation Model for Bearing Capacity of Steel-CFRP Composite Pipeline Under Internal Pressure," *Heliyon* 10 (2023): e27238.

29. S. Soveiti and R. Mosalmani, "Mechanical Behavior of Buried Composite Pipelines Subjected to Strike-Slip Fault Movement," *Soil Dynamics and Earthquake Engineering* 135 (2020): 106195.

30. ALA, *Guidelines for the Design of Buried Steel Pipes* (American Lifelines Alliance, 2005).

31. PRCI, *Guidelines for the Seismic Design and Assessment of Natural Gas and Liquid Hydrocarbon Pipelines* (Pipeline Research Council International, 2004).

32. D. Wijewickreme, D. Honegger, A. Mitchell, and T. Fitzell, "Seismic Vulnerability Assessment and Retrofit of a Major Natural Gas Pipeline System: A Case History," *Earthquake Spectra* 21, no. 2 (2005): 539–567.

33. A. M. Gresnigt, "Plastic Design of Buried Steel Pipelines in Settlement Areas," *Heron* 31, no. 4 (1986): 1–113.

34. Kratos, "Kratos C-Plate Technical Datasheet, Kordsa Composite Technologies Center of Excellence, Turkey," https://kratosreinforcement.com/wp-content/uploads/2023/05/Kratos_Structural-Reinforcement-TDS_TR_CPLATE.pdf.

35. ASTM D3039/D3039M-08, *Standard Test Method for Tensile Properties of Polymer Matrix Composite Materials* (ASTM International, 2008).

36. ASTM D790-17, *Standard Test Methods for Flexural Properties of Unreinforced and Reinforced Plastics and Electrical Insulating Materials* (ASTM International, 1997).

37. ASTM D-792, *Standard Test Methods for Density and Specific Gravity (Relative Density) of Plastics by Displacement* (ASTM International, 1991).

38. P. D. Soden, M. J. Hinton, and A. S. Kaddour, "Lamina Properties, Lay-Up Configurations and Loading Conditions for a Range of Fibre Reinforced Composite Laminates," in *Failure Criteria in Fibre Reinforced Polymer Composites: The World-Wide Failure Exercise*, ed. M. J. Hinton, A. S. Kaddour, and P. D. Soden (Elsevier Ltd, 2004), 30–51.

39. M. M. Shokrieh and L. B. Lessard, "Progressive Fatigue Damage Modeling of Composite Materials, Part II: Material Characterization and Model Verification," *Journal of Composite Materials* 34, no. 13 (2000): 1081–1116.

40. P. Vazouras, S. A. Karamanos, and P. Dakoulas, "Finite Element Analysis of Buried Steel Pipelines Under Strike-Slip Fault Displacements," *Soil Dynamics and Earthquake Engineering* 30, no. 11 (2010): 1361–1376.

41. P. Vazouras, S. A. Karamanos, and P. Dakoulas, "Mechanical Behavior of Buried Steel Pipes Crossing Active Strike-Slip Faults," *Soil Dynamics and Earthquake Engineering* 41 (2012): 164–180.

42. E. Uckan, B. Akbas, J. Shen, W. Rou, F. Paolacci, and M. O'Rourke, "A Simplified Analysis Model for Determining the Seismic Response of Buried Steel Pipes at Strike-Slip Fault Crossings," *Soil Dynamics and Earthquake Engineering* 75 (2015): 55–65.